Quantification for Food Inspection enabled by Hyperspectral Imaging System and Machine Learning

Un Jeong Kim (ujjane.kim@samsung.com)
Samsung Advanced Institute of Technology https://orcid.org/0000-0003-2799-8168

Suyeon Lee
Samsung Advanced Institute of Technology

Hojung Kim
Samsung Advanced Institute of Technology/Samsung Electronics Corporation

Hyochul Kim
Samsung Advanced Institute of Technology

Seok In Kim
School of Integrative Engineering, Chung-Ang University

Young-Geun Roh
Samsung Advanced Institute of Technology

Hyungbin Son
School of Integrative Engineering, Chung-Ang University

Jeong Su Han
Samsung Electronics

Junhoe Choi
Samsung Electronics

Sungmin kim
Samsung Electronics

Soo Eon Kim
Samsung Electronics

Inho Hwang
Chungnam National University

Yeonsang Park
Chungnam National University https://orcid.org/0000-0002-9746-8026

Seokho Yun
Samsung Advanced Institute of Technology

Physical Sciences - Article

Keywords:

Posted Date: April 14th, 2023

DOI: https://doi.org/10.21203/rs.3.rs-2725086/v1

Abstract

Several important sensory physical quantities exist but are difficult to quantify, including food freshness. With the aid of a hyperspectral imaging system (HIS) and machine learning (ML), meat freshness is converted into a measurable physical quantity, i.e., freshness index (F. I.), in this study. F. I. is defined from meat fluorescence, which has a strong correlation with bacterial density, using a line-scan-type HIS stimulated at 365 nm. Combined with ML techniques, hyperspectral images are processed more efficiently. By employing linear discriminant and quadratic component analyses for hyperspectral images, F. I. can be estimated from its decision boundary after hyperspectral images are taken at an unknown freshness state. Advanced sensing versatility utilized by computational sensing systems allows hyper-personalization and hyper-customization of human life with the aid of home appliances and smartphones.

Introduction

In various domains of research and business, the statistical analysis of big data has gained prominence owing to the enormous volume of big data requiring analysis within a progressively shortened period. By establishing a correlation between raw sensing data and ambiguously defined physical quantities, researchers have recently reported a growing versatility in the functionality and enhanced performance of traditional sensors when combined with machine learning (ML) based statistical analysis.[1–7] Furthermore, the utilization of advanced sensing versatility by computational sensing systems through different home appliances enables hyper-personalization and hyper-customization of human everyday life including food inspection, healthcare, and beauty care.[8–10]

With the steadily rising consumption of meat along with gastronomic flavor, its freshness and aging have emerged as the most intriguing quality control factors for food inspection. Defining the freshness or aging degree of meat as a physical quantity is intriguing, ambiguous, and strongly influenced by personal preference. Currently, standard techniques for the evaluation of meat freshness or its aging degree are mostly destructive, non-portable, expensive, and difficult to access by general users.[11,12] Thus, optical inspection techniques such as the reflectance of UV–Vis–NIR from meat surfaces have been investigated over several decades. [13–15] However, several approaches rely on extracting the degree of freshness without understanding the underlying mechanism related to specific molecular changes in freshness, which has rendered the results unreliable and unreproducible.[13–15] To investigate the freshness of pork meat, suitable biomarkers such as collagen, reduced nicotinamide adenine dinucleotide (NADH), and flavin have been deemed suitable.[16,17] Studies have monitored the ~ 390, 460, and 525 nm fluorescence as a function of time from pork specimens stored at room and refrigerator temperatures (4 ^{o}C), when stimulated by a 340 nm light emitting diode (LED) for up to three days.[16,17] However, statistical and areal map studies of meat freshness in specimens have not been performed based on the correlation between meat freshness and fluorescence from biomarkers. Thus, a hyperspectral imaging system (HIS) is

considered suitable for extracting invisible information on food inspection by imaging morphological and spectroscopic data collected from macroscale meat samples through ML grafting.

In this study, meat freshness is monitored using HIS and ML as proof-of-concept. It can be clearly distinguished not by an RGB camera but spectral information from HIS. By combining HIS with ML, meat freshness can become a tangible physical quantity for applications in daily life. This study can be applied in the domain of smartphone business, which would allow people to test and evaluate meat readily at any place and situation.

Acquisition of Hyperspectral Data Cube and Evaluation of Meat Freshness by ML

Figure 1 shows the entire process behind obtaining data cubes using HIS and ML for identifying meat freshness. In this study, the line-scan and snapshot types of HIS were used to image the morphology and spectral information of meat specimens. A line-scan-type HIS was designed to move 365 nm LED arrays, while a long rectangular window was developed to excite and collect fluorescence signals over the meat specimens. The fluorescence signal transported to a commercially available grating was collected in the form of 3D (one spectral dimension and two spatial dimensions) hyperspectral data cube, as shown in **Fig. 1**. For the snapshot-type HIS, Fabry–Perot filters were fabricated periodically on a complementary metal–oxide–semiconductor (CMOS) image sensor, which worked in the range 380–840 nm (see methods). The schematics for line-scan and snapshot types of HIS are shown in in **Extended Data Figs. 1 and 2**, respectively. High spectral and spatial resolution of the line-scan-type HIS is beneficial for investigating parameters correlated with meat freshness from the fluorescence spectrum. For details on the scanning area and spatial resolution for both types of HIS, see methods. Meat freshness could be extracted from the hyperspectral images by processing data efficiently. Particularly, ML on a hyperspectral data cube with the merit of data size obtained by snapshot-type HIS, based on fundamental studies on line-scan-type HIS, was conducted to evaluate the information on meat freshness.

Hyperspectral images of the meat surface were decomposed into a series of spectral bands (λ_1, λ_2, λ_3, λ_4, ...), forming a hyperspectral data cube. The full spectrum of each local point was constructed by combining intensity and wavelength in the vertical direction. Typical fluorescence spectra of fresh and rotten meat specimens are shown in **Extended Data Fig. 3a** and **b**. The broadband from NADH at 490 nm and its enhancement in intensity with lowered freshness agreed with those observed in previous studies.[17,18] Conversely, the sharp peak at ~ 600 nm appeared to have a relation with myoglobin, which exists inside living cells of mammals and is related to their breathing activity. The reference spectra of NADH and myoglobin purchased from Aldrich Inc. were exceptionally similar to those of meat and are shown in in **Extended Data Fig. 3c** and **d**, respectively.

Traditional Analysis of Meat Freshness and 2D Freshness Index Map

To understand the morphological and chemical changes in meat specimens as a function of refrigerator storage time ($T \approx 4\ ^{o}C$), RGB images illuminated with white LED and hyperspectral images of

fluorescence excited by 365 nm were captured by a digital camera and line-scan-type HIS, respectively. The process was conducted on the same piece of specimen under the same conditions for approximately 17 days and the results are shown in **Fig. 2a** and **b**. The meat specimens were packaged in polyethylene (PE) wraps to avoid contamination and other handling issues. The RGB images of the meat specimens as a function of storage time were analyzed using the CIELAB color space, referred to as *L*a*b**, where *L** represents lightness, *a** represents green–red opponent colors with negative and positive values toward green and red, respectively, and *b**denotes blue–yellow opponents with negative and positive values toward blue and yellow, respectively. The distributions of *a** and *b** values, represented by red and yellow bars, are displayed on the right side for each RGB image, while their average values are indicated by red and yellow dots in the guideline, respectively. With increase in storage time, both *a** and *b** values merged to 10 starting from the 7th day, implying that the color of meat turned less reddish and yellowish. In addition, distinguishing the state of meat freshness after the 7th day was not possible. Another type of RGB images defined by "RGB^{hyper}" was obtained by transforming hyperspectral images of meat fluorescence via the CIEXYZ color space, as shown in **Fig. 2b**, where the representative fluorescence spectrum of each storage day is displayed on the right side. With longer storage time, the relative intensity of NADH located at ~ 490 nm against 600 nm increased. F. I. was defined as

$$\mathrm{F.I.} = (I_N - I_M) / (I_N + I_M)$$

1

where I_N and I_M are the intensities of NADH and myoglobin peaks deconvoluted from the fluorescence spectrum, shown by the blue and pink shaded areas, respectively. Figure 2**c** shows a 2D map of F. I. for each storage day, while **Fig. 2d** shows the average F. I. value of each hyperspectral image, which increased monotonously up to the 10th day and finally saturated. The number of bacteria per unit area (CFU/cm^2) (N_{bac}) measured using the standard method (see methods) gradually increased on a logarithmic scale, as shown in **Fig. 2e**, where the pink shaded area indicates the inedible state of meat at N_{bac} > 10^7 (CFU/cm^2)[17]. Thus, F. I. was confirmed to have a strong correlation with meat freshness. However, the CIELAB color space analysis of the RGB images confirmed that meat freshness could not be distinguished after the 7th day of storage, although meat remained edible at N_{bac} < 10^7 (CFU/cm^2). The correlation among N_{bac}, storage date (*d*), and F. I. was obtained by fitting the experimental data shown in **Fig. 2d** and **e** using a relation defined as

$$\log(N_{bac}) = 2.6\sqrt{d + 6.4} - 3.4$$

2

$$F.I. = 0.066\,(\log(N_{bac}) + 2.5)$$

3

.

Using these functions, guidelines were added to the experimental data by applying a width of ± 1.0 and ± 0.1 in **Fig. 2d** and **e**. According to Eq. (3), F. I. > 0.63 for the inedible state and is indicated as the pink shaded area in **Fig. 2d**.

The F. I. of the meat specimens, one stored in a refrigerator and the other in a freezer, was monitored as a function of storage time to prove the representativeness of meat freshness at unknown storage or commercial distribution channel history. Predictably, the F. I. values of the sample stored in the refrigerator increased gradually to approximately 0.7, but those of the sample stored in the freezer remained at approximately 0.55, as shown in **Fig. 2f**. At the first stage, the initial increase in the F. I. value for the frozen meat could be attributed to the structural changes in the meat specimen or an actual increase in N_{bac} before freezing.

The color of meat specimens is particularly related to the oxidation of myoglobin. Meat is bright red, which looks fresh to the human eyes, owing to iron oxidation at the center of the heme ring in myoglobin molecules by attaching oxygen or water molecules. When the meat specimen is vacuum-packaged, its color turns dark brown, which looks stale to the human eye. The freshness of PE wrap and vacuum-packaged meat specimens is investigated as a function of storage time using the F. I. and a*/b* values from hyperspectral and RGB images, respectively. The color of the meat specimen was darker even on the 0th day, as shown in **Fig. 3**, due to the desorption of oxygen molecules from myoglobin on the meat surface during vacuum packaging. Figure 3**a** shows an RGB image under white light captured by a digital camera, an RGB^{hyper} image, and the F. I. map of a vacuum-packaged meat specimen on the 0th day. On the 0th day, *a** and *b** for the vacuum-packaged meat were distributed in a range, shown in **Fig. 3b**, similar to that of inedible meats, and they remained similar until the 12th day, as shown in **Extended Data Fig. 4a**. The values of F. I., *a**, and *b** were monitored as a function of storage time for both vacuum- and PE-packaged samples, and the results are presented in **Fig. 3c and d**, respectively. N_{bac} was monitored in the PE-packaged meat specimen stored together with the vacuum-packaged meat specimen (**Extended Data Fig. 4b**). N_{bac} for the present batch increased rapidly when compared to that shown in **Fig. 2** because of different environmental conditions, including weather, preparation process, and distribution channel history. The representative fluorescence spectra on the 0th and 12th day are shown in **Extended Data Fig. 4c**. The PE-packaged meat exhibited a gradual increase in the F. I. value, which was similar to that of N_{bac}, as shown in **Fig. 3c** due to exposure to air. However, the F. I. value of the vacuum-packaged meat was maintained approximately to the 12th day because the meat stayed fresh by preventing oxygen adsorption on its surface. The freshness of the vacuum packaged meat was verified through the hyperspectral image of the meat fluorescence and its F. I., as shown in **Extended Data Fig. 4d**. The gray shaded area in **Fig. 2d** and **e** represent the guidelines that were calculated using Eqs. (2) and (3). The slight discrepancy between the experimental data (black dots) illustrated in **Fig. 3c** may have originated from the different relative ratios of fat and flesh contents in the meat specimens used, as shown in **Fig. 2a**. Since the characteristic band of fatty acids is located in a wavelength range similar to that of NADH, Eqs. (2) and (3) were modified to fit F. I. with a higher accuracy by excluding the areas of fat while calculating F. I..[19] On the 0th day, the vacuum-packaged meat in **Fig. 3b** exhibited relatively lower average

values of *a** and *b** when compared to those of the PE-packaged specimen in **Fig. 2a**. *a** and *b** are shown to be < ~ 22 and < ~ 30, and < ~ 30 and < ~ 40 for vacuum packaged and PE wrapped specimen, respectively. With prolonged storage time, the mean values of *a** and *b** of the PE-packaged meat tended to decrease, while they remained almost constant for the vacuum-packaged specimen, as shown in Fig. Figure 3**d**. From the 0th to the 12th day, the mean values of *a** and *b** changed slightly from 13.7 to 12.5 and from 7.6 to 4.7 for the vacuum-packaged meat, respectively. Furthermore, the color of meat could be influenced by various factors such as its freshness, pH, part of meat, and nutritional state. However, larger differences between the F. I values of the PE- and vacuum-packaged specimens than *a** and *b** were observed. Thus, the results suggest that meat freshness can be classified more clearly by using hyperspectral image sensors than by RGB image sensors. Expectedly, meat freshness can also be distinguished by imaging meat fluorescence under a 365 nm LED using an RGB camera. We simulated the RGB image of meat fluorescence by converting the hyperspectral image into RGB^{hyper} images as a function of the storage time. We observed that the *a** and *b** values of the RGB^{hyper} images did not change sensitively within the edible state (≤ 7th day of storage), as shown in **Extended Data Fig. 5**. Thus, hyperspectral imaging was confirmed to be a powerful tool for discerning meat freshness against RGB images taken under white or 365 nm LED. Since the freshness stage of meat is not easily accessible to consumers, the proper analysis tool needs to be devised for precise freshness evaluation.

In an experiment, four types of packaging materials, listed in table S1, were investigated to understand their influence on the fluorescence spectrum. The results are shown in **Extended Data Fig. 6a** and **b**. PE and PVC wrap or zipper bags produced unnoticeable fluorescence signals, while vacuum packaging material produced a non-negligible intensity of broad fluorescence at approximately 470 nm. However, the condition was magnified more than 20 times as shown in **Extended Data Fig. 6a**, where 5 s integration with two layers was performed as compared with the experimental condition of 400 ms to obtain fluorescence from the meat specimen. On packaging the meat in PE or PVC wrap and zipper bags, the shape of the fluorescence spectrum was maintained while its intensity decreased, as shown in **Extended Data Fig. 6b**. The overall line-shape of the fluorescence was independent of the packaging material. This result indicates that fluorescence spectroscopy can be applied in daily life to analyze meat freshness when commercial food packaging materials are used.

Hyperspectral Imaging and ML for Meat Freshness by Snapshot-type HIS

Furthermore, a 16-channel(CH) snapshot-type HIS was fabricated and Fabry–Perot filters were formed periodically on a CMOS image sensor operating in the 380–840 nm range while including a blank channel. To optimize transmission and its resonance wavelength, alternative TiO_2 and SiN films with variable thicknesses were stacked vertically along with Cu or Al reflectors at the top and bottom, behaving as a Fabry–Perot filter. The final characteristic transmission curves shown in **Fig. 4a** were obtained by multiplying the quantum efficiency (QE) of the CMOS image sensor and transmission of each filter. Figure 4**b** shows the hyperspectral image of fluorescence from the meat specimen supported by a black Styrofoam tray, excited by 365 nm LEDs. The image was demosaiced into each CH, as shown on the right side of **Fig. 4b**, where the enlarged CH distribution of the small yellow square in the hyperspectral image

is shown on the right-hand side. Hyperspectral images from the same meat specimen were taken as a function of storage time. For the 0th and 15th day, two representative fluorescence spectra from the fresh and rotten states of the meat specimen taken by the snapshot-type HIS, respectively, are shown in **Fig. 4c**. Comparatively, a large enhancement at approximately 500 nm was observed on the 15th day as opposed to the 0th day. Thus, the results were consistent with those obtained from the line-scan-type HIS, as illustrated in **Fig. 2**. ML can be applied to reduce the dimensions of hyperspectral data cubes and to extract features related to meat freshness from hyperspectral images. The reduction in data dimensionality can maximize the efficiency of computing resources, such as computing time and memory. Moreover, the risk of overfitting data resulting from a complicated analysis model can be reduced, and the dimension reduction can prove to be advantageous for the ease of data interpretation. Among various algorithms available for dimension reduction, principal component analysis (PCA) and LDA are commonly used.[20,21] LDA is opted for dimensionality reduction of hyperspectral data from 11 to 2 dimensions (indicated by $\mathrm{LDAcomponent}_1$ and $\mathrm{LDAcomponent}_2$ in **Fig. 5a**). Four long-wavelength CHs and one blank CH were initially excluded out of the 16 CHs that did not convey information on the fluorescence signal from the meat specimen. The raw intensity profiles of the remaining 11 CHs as a function of wavelength were standardized by their mean value and standard deviation. Furthermore, dimensionality reduction from 11 to 2 dimensions was conducted by subtracting the channel-dependent constant ($\bar{x_j}$) from value of each CH (x_j), followed by the multiplication of two coefficients ($\mathrm{scalingfactor}_1$ and $\mathrm{scalingfactor}_2$), which were determined using the LDA method. The data points are shown in **Extended Data Fig. 7**. Here,

$$\mathrm{LDAcomponent}_i = \sum_{j=1}^{11} \mathrm{scalingfactor}_j \left(x_j - \bar{x_j}\right), i = 1, 2$$

4

LDA component$_1$ was plotted against LDA component$_2$ of the hyperspectral images of meat as a function of storage time, as illustrated in **Fig. 5a**. With longer durations of storage time, highly scattered data were gradually merged to the negative values of the LDA component$_1$, where each dot was extracted from dimensionality reduction using LDA. Even on the 0th day, the negative values of LDA component$_1$ appeared to originate from the fat tissues whose fluorescence was similar to that of NADH. The decision or evaluation boundaries of F. I. produced by QDA are shown in **Fig. 5b** as contour plots.[22] Information on F. I., averaged over each hyperspectral image by line-scan-type HIS as reference data, and hyperspectral images taken by snapshot-type HIS were obtained for identical meat specimen as a function of storage time. Since the average value of F. I. of the meat specimen was initially known from the analysis of line-scan-type HIS, QDA was adopted to obtain decision boundaries of the F. I. for the two LDA components under supervised learning. By hyperspectral imaging of meat fluorescence and extracting two components through LDA, the value of F. I. was estimated using the decision boundary contour plot shown in **Fig. 5b**. RGB^{hyper} images were constructed from snapshot hyperspectral images, as shown in the upper row of **Fig. 5c**. Gradually, the image turned bluish. The values of R, G, and B were calculated by

averaging the intensities of the three channels at (630 nm, 670 nm, 690 nm), (520 nm, 540 nm, 575 nm), and (430 nm, 460 nm, 495 nm), respectively. The F. I. maps constructed from the hyperspectral images by the LDA and QDA are shown in the lower panel of **Fig. 5c**. Thus, gradual changes in the F. I. values of the meat specimens were visualized as a function of storage time.

Furthermore, ML analysis with snapshot-type hyperspectral images was applied to vacuum-packaged meat for comparison with the PE-wrap-packaged meat. The results are presented in **Extended Data Fig. 8**. For the vacuum-packaged meat, the RGB^{hyper} images converted from the hyperspectral images and its F. I. map were compared on the 0th and the 28th day. The F. I. distribution up to the 28th day remained similar to the initial state, as shown in **Extended Data Fig. 8a**. The dependency of the F. I. values of PE- and vacuum-packaged meat specimens on storage time, obtained by line-scan-type and snapshot-type HIS, is shown in **Extended Data Fig. 8b**. Irrespective of the HIS type, the time-dependent behavior of F. I. was quite similar, both qualitatively and quantitatively

Despite low spatial and spectral resolution compared to line-scan-type HIS, the snapshot-type HIS offered competitive advantages in several aspects, such as cost effectiveness and efficiency of computing resources. Using this methodology, a smartphone installed with a hyperspectral camera can be used to capture both outer appearance and hyperspectral images of meat at any place to determine meat freshness. To make hyperspectral cameras more powerful in business domains, proper ML-based algorithms have to be developed to find the true color, spectrum, and applications of the objects under interest.

Discussions

In this study, hyperspectral imaging technique has been successfully applied to confirm meat freshness and to map freshness index in two dimensions by adopting ML. The features correlated with the freshness of meat were studied by line-scan-type HIS incorporated with conventional gratings having high spatial and spectral resolution. The F.I. value of the meat specimen was defined from the fluorescence spectrum and the value was compared with bacterial density. Based on these fundamental studies, ML was applied to the hyperspectral images captured by the snapshot-type HIS to identify meat freshness. LDA was adopted to efficiently reduce data dimensionality for extracting the features of meat freshness. Furthermore, QDA was applied to construct the decision boundaries of F. I. under supervised learning against LDA components. After the hyperspectral images of meat at an unknown freshness state were taken, LDA components were determined, and then the value of F. I. was estimated from the decision boundary, which lead to an approximate bacterial density. This work demonstrates that ambiguous physical quantities such as meat freshness can be substantialized by HIS and ML. Our findings can be applied to smartphone which will open a new business model toward hyper-personalization and hyper-customization of human life.

Methods

Hyperspectral imaging system (HIS) and Measurement

Line-scan type: A commercial spectrometer composed of a grating and an image sensor from Ximea Corp. was installed in the line-scan-type HIS. The distance (*h*) between the meat specimen and the 365 nm LEDs was maintained at 2.5 cm. Using 28 LEDs, approximately 37 mW was uniformly applied over the meat specimen. A two-dimensional hyperspectral image was obtained by collecting the spectrum from the thin rectangular window along the x-axis with an exposure time of 400 ms at each step. The length in the perpendicular direction (*l*) against the thin rectangular window along the y-axis could be varied. The y-axis resolution could be varied by varying the distance between *l* and *h*. The lateral resolution of the x-axis was strongly dependent on *h*. The size of the images was 972·55 pixels, while the spatial resolution was found to be 0.0988 and 0.408 mm/pixel along the x- and y-axes at *h* = 2.5 cm, respectively.

Snapshot type: The distance between the meat specimen and hyperspectral image sensor was maintained at 23 cm. A lens of F/1.2 and f = 6 mm, purchased from Fujinon (DF6HA-1B), was used to image an area of approximately 104·8.4 mm. The CMOS image sensor had 2608·1960 pixels with a size of 1.4 μm per pixel. Each pixel conveyed 10 bits of information. Each channel was composed of two pixels. Therefore, the spatial size of the data cube was 326·245 after the demosaicing process. Figure 4 shows an image of a specimen with 140×140 pixels. The measurement conditions were set to 1 s exposure time, 16 s analog gain, and 1 s digital gain.

Imaging RGB by digital camera

The RGB images of the meat specimen were obtained in a small box using a digital camera (DSC-RX100, Sony Corp., Seoul, Korea). Simultaneously, a reference white plate (MINOLTA calibration plate) was placed right next to the meat specimen. A white LED was illuminated through a window placed 20 cm from the meat specimen.

Preparation of meat specimen

Loafs of beef sirloin were purchased from a store in Suwon, Korea Federation of Livestock Cooperatives. A loaf was sliced into pieces of 5·5·1.5 cm. Each piece of meat specimen was placed on a black Styrofoam tray, which was sanitized with alcohol and packaged in a PE wrap, to image the hyperspectral imaging as a function of time. Additional pieces of the meat specimen were vacuum packaged. Five pieces of the meat specimen were prepared for N_{bac} measurement for each storage time. Two of the five pieces were checked with hyperspectral imaging at each storage time. They were consumed for one N_{bac} measurement. Three additional pieces of the meat specimen packaged in a PE wrap were kept in the refrigerator and measured by hyperspectral imaging as a function of storage time.

Measuring bacterial density (N_{bac} (CFU/unit)) and temperature

General bacteria were collected by rubbing both sides of the meat specimen surface with a swab (3M Pipette Swab, MN, St. Paul, MN, USA) a given number of rubbing times. The rubbed swab was rinsed in 1 mg of phosphate-buffered saline (PBS), which was further diluted 10 times. Two sets of 1 ml of the diluted solution containing the general bacteria were dropped onto a petrifilm, which was dried at 35 ± 1°C for 48 ± 2 h. The number of red colonies was then counted. The final N_{bac} value was obtained by multiplying the counted number by 10. As a reference, a clean PBS solution was compared with a PBS solution containing the general bacteria collected from the meat surface.

The temperatures of the refrigerator (T^{ref}), freezer (T^{fre}), and national weather service (T^{nat}) were registered to understand the possible correlation with the increasing value of N_{bac}. The results shown in Figs. 2(A–C) were measured on May 12–29, 2020, at T^{ref} = 2.2°C and T^{nat} =13.5–20.0°C, and those in Fig. 3 were measured from September 9 to 21, 2020, at T^{ref} = 2.9 ℃ and T^{nat} =18.3–22.6 ℃. The results shown in Fig. 2(D) were measured from January 22 to February 10, 2021, at T^{ref} = 3.5 ℃, T^{fre} = − 4 ℃, and T^{nat} = − 8.1–7.9 ℃. The results shown in Figs. 4 and 5 were measured from May 14 to 29, 2021, at T^{nat} = 14.8–20.9 ℃ for the PE-wrapped specimen, while for the vacuum-packaged specimen, the results were measured from May 14 to June 11, 2021, at T^{nat} = 14.8–20.9 ℃.

Declarations

Data availability

The data that support the findings of this study are available from the corresponding author upon reasonable request.

Code availability

The computer codes used in this study are available from the corresponding author upon reasonable request.

Acknowledgments

National Research Foundation of Korea (NRF) grant NRF-2021R1F1A1062182 (PV, YP)

National Research Foundation of Korea (NRF) grant NRF-020R1A6A1A03047771 (PV, YP)

Korea Institute for Advancement of Technology (KIAT) grant (PV, YP)

Author Contributions

U.J.K, S.L, and H.S. conceived and designed the research. U.J.K. and S.K conducted optical measurements. H.K., Y.R., and Y.P. fabricated the 128CH filter arrays and measured the corresponding transmissions. S.L. devised and carried out the machine algorithm. H.S. designed and fabricated the line scan type HIS. suggested experimental procedures and methods. J.S.H., J.C., S.K. and S.E.K and S.Y. had

valuable discussions. M.J.C. selected the list of drugs. U.J.K. and S.L. wrote the manuscript. All authors reviewed the manuscript.

Competing interests

The authors declare no competing interests.

Additional information

Supplementary information is available for this paper at http://doi.org/xxx.

Reprint and permissions information is available at www.nature.com/reprints.

Correspondence and requests for materials should be addressed to U. J. K. (ujjane.kim@samsung.com).

References And Notes

1. Jiang, T., Li, C., He, Q. & Peng, Z. K. Randomized resonant metamaterials for single-sensor identification of elastic vibrations. *Nat Commun* **11**, (2020).
2. Feng, C., Au, W. S. A., Valaee, S. & Tan, Z. Received-signal-strength-based indoor positioning using compressive sensing. *IEEE Trans Mob Comput* **11**, 1983–1993 (2012).
3. Zhang, X. *et al.* MEMS-based super-resolution remote sensing system using compressive sensing. *Opt Commun* **426**, 410–417 (2018).
4. Shi, Q. *et al.* Deep learning enabled smart mats as a scalable floor monitoring system. *Nat Commun* **11**, (2020).
5. Golestani, N. & Moghaddam, M. Human activity recognition using magnetic induction-based motion signals and deep recurrent neural networks. *Nat Commun* **11**, (2020).
6. Ballard, Z., Brown, C., Madni, A. M. & Ozcan, A. Machine learning and computation-enabled intelligent sensor design. *Nat Mach Intell* **3**, 556–565 (2021).
7. Lee, Y. *et al.* Flexible Pyroresistive Graphene Composites for Artificial Thermosensation Differentiating Materials and Solvent Types. *ACS Nano* **16**, 1208–1219 (2022).
8. Hadoux, X. *et al.* Non-invasive in vivo hyperspectral imaging of the retina for potential biomarker use in Alzheimer's disease. *Nat Commun* **10**, (2019).
9. Joung, H. A. *et al.* Point-of-Care Serodiagnostic Test for Early-Stage Lyme Disease Using a Multiplexed Paper-Based Immunoassay and Machine Learning. *ACS Nano* **14**, 229–240 (2020).
10. Kim, U. J. *et al.* Spectral Barcode for Drug Classication Enabled with a Smartphone Raman Spectrometer. (2023) doi:10.21203/rs.3.rs-2435626/v1.
11. Lee, Y. J. & Ko, K. S. Effects of extract of lactic acid bacteria culture media on quality characteristics of pork loin and antimicrobial activity against pathogenic bacteria during cold storage. *Journal of the Korean Society of Food Science and Nutrition* **45**, 1476–1480 (2016).

12. Seol, K.-H., Kim, K. H., Kim, Y. H., Youm, K. E. & Lee, M. Effect of temperature and relative humidity in refrigerator on quality traits and storage characteristics of Pre-packed Hanwoo loin. *Korean Journal of Agricultural Science* **41**, 415–424 (2014).
13. Andrés, S. *et al.* Prediction of sensory characteristics of lamb meat samples by near infrared reflectance spectroscopy. *Meat Sci* **76**, 509–516 (2007).
14. McManus, C. *et al.* Infrared thermography in animal production: An overview. *Computers and Electronics in Agriculture* vol. 123 10–16 Preprint at https://doi.org/10.1016/j.compag.2016.01.027 (2016).
15. Kucha, C. T., Liu, L. & Ngadi, M. O. Non-destructive spectroscopic techniques and multivariate analysis for assessment of fat quality in pork and pork products: A review. *Sensors (Switzerland)* vol. 18 Preprint at https://doi.org/10.3390/s18020377 (2018).
16. Pu, Y., Wang, W. & Alfano, R. R. Optical detection of meat spoilage using fluorescence spectroscopy with selective excitation wavelength. *Appl Spectrosc* **67**, 210–213 (2013).
17. Wu, B., Dahlberg, K., Gao, X., Smith, J. & Bailin, J. Rapid measurement of meat spoilage using fluorescence spectroscopy. in *Imaging, Manipulation, and Analysis of Biomolecules, Cells, and Tissues XV* vol. 10068 1006820 (SPIE, 2017).
18. Ministry of Food and Drug Safety of Korea. KFDA. Food code.
19. Aït-Kaddour, A. *et al.* Potential of fluorescence spectroscopy to predict fatty acid composition of beef. *Meat Sci* **113**, 124–131 (2016).
20. Su, J., Yi, D., Liu, C., Guo, L. & Chen, W. H. Dimension reduction aided hyperspectral image classification with a small-sized training dataset: Experimental comparisons. *Sensors (Switzerland)* **17**, (2017).
21. Beatriz P. P. Garcia-Salgado, Volodymyr I. Ponomaryov, Sergiy N. Sadovnychiy & Rogelio Reyes-Reyes. Efficient dimension reduction of hyperspectral images for big data remote sensing applications. *J Appl Remote Sens* **14**, (2020).
22. Zhao, B., Ulfarsson, M. O., Sveinsson, J. R. & Chanussot, J. Unsupervised and supervised feature extraction methods for hyperspectral images based on mixtures of factor analyzers. *Remote Sens (Basel)* **12**, (2020).

Figures

Figure 1

Schematics of the full process required to obtain hyperspectral data cube and evaluation using ML for food inspection. Two hyperspectral imaging systems are incorporated for hyperspectral data cube acquisition.: 1) line-scan-type HIS installed with commercial grating for high spatial and spectral

resolution and 2) snapshot-type HIS for efficient computation resources. ML is conducted to extract F. I. values from the hyperspectral data cubes for food inspection.

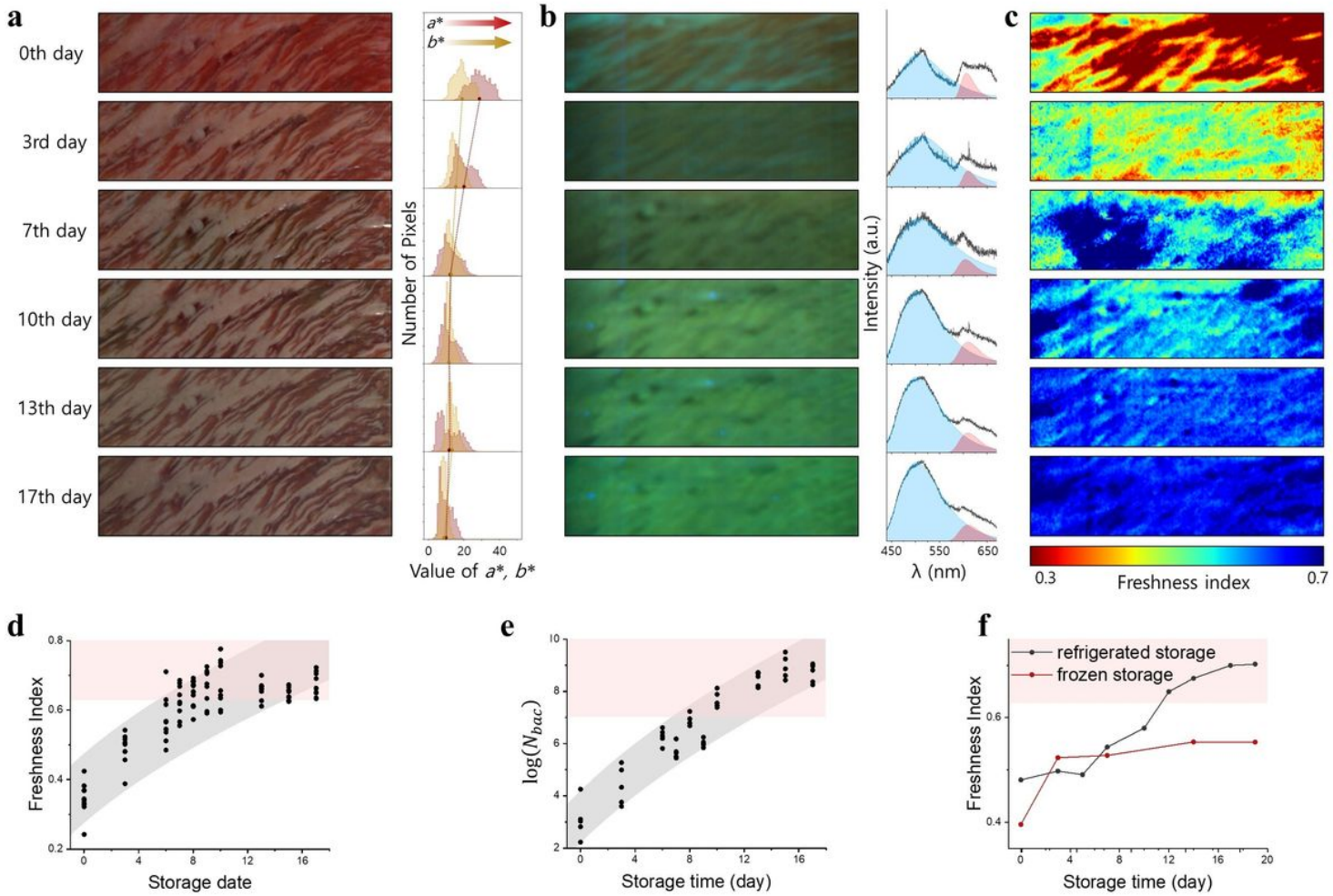

Figure 2

Tracking meat freshness and two-dimensional maps of F. I. of meat specimen. (A) RGB images of meat specimen taken by a digital camera under white light illumination and the distribution of *a** and *b**. Red and yellow solid lines are used to track the average values at each stage. (B) RGB images converted from hyperspectral images of fluorescence signals collected by line-scan-type HIS and its representative spectrum on the right are displayed as a function of storage time. The same area of the meat specimen is monitored for the RGB and hyperspectral images of fluorescence. (C) Two-dimensional map of the F. I. of the meat specimen are reconstructed based on the hyperspectral data cube in (B). (D) Average F. I. values for each hyperspectral image and (E) bacteria density (N_{bac}) are plotted as a function of storage time. The pink shaded area indicates inedible state of meat $N_{bac} > 10^7$ (CFU/cm^2) and corresponding F.I. > 0.63. (F) Storage time dependent F. I. of meat specimens stored in refrigerator at T = 4 ^{o}C (black dot) and freezer (red dot).

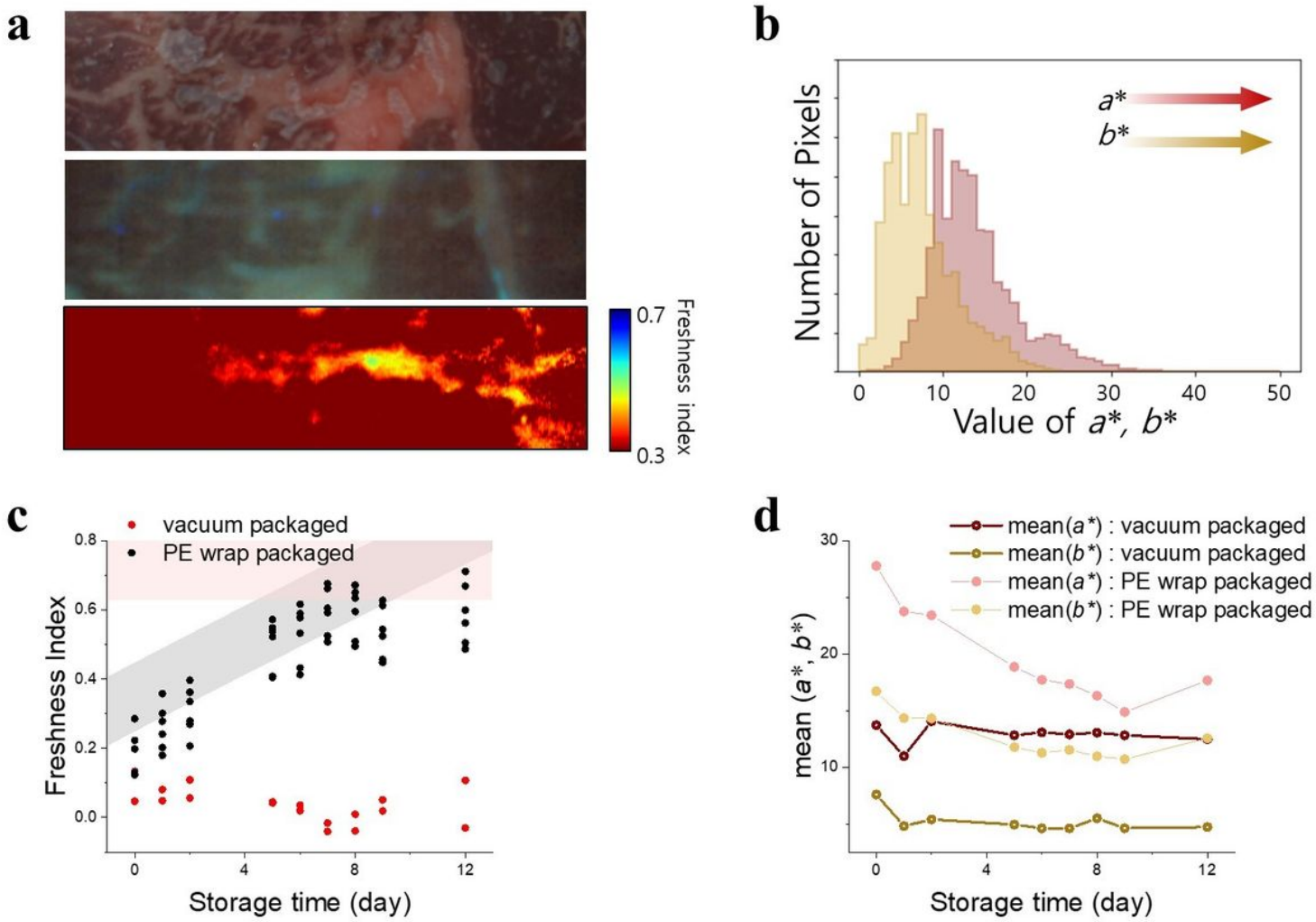

Figure 3

Freshness of the vacuum-packaged meat specimen. (A) RGB image taken by a digital camera, transformed from the hyperspectral image of the vacuum-packaged meat specimen and its F.I. on the 0th day. (B) Distribution of *a** and *b** values of the RGB images take by a digital camera in (A). (C) F. I. of the vacuum-packaged (red dot) and PE-wrap-packaged (black dot) meat specimen as a function of storage time. Six and two pieces of vacuum-packaged and PE-wrap-packaged meat specimen are investigated, respectively. (D) Mean *a** and *b** values of the vacuum-packaged and PE-wrap-packaged meat specimen as a function of storage time.

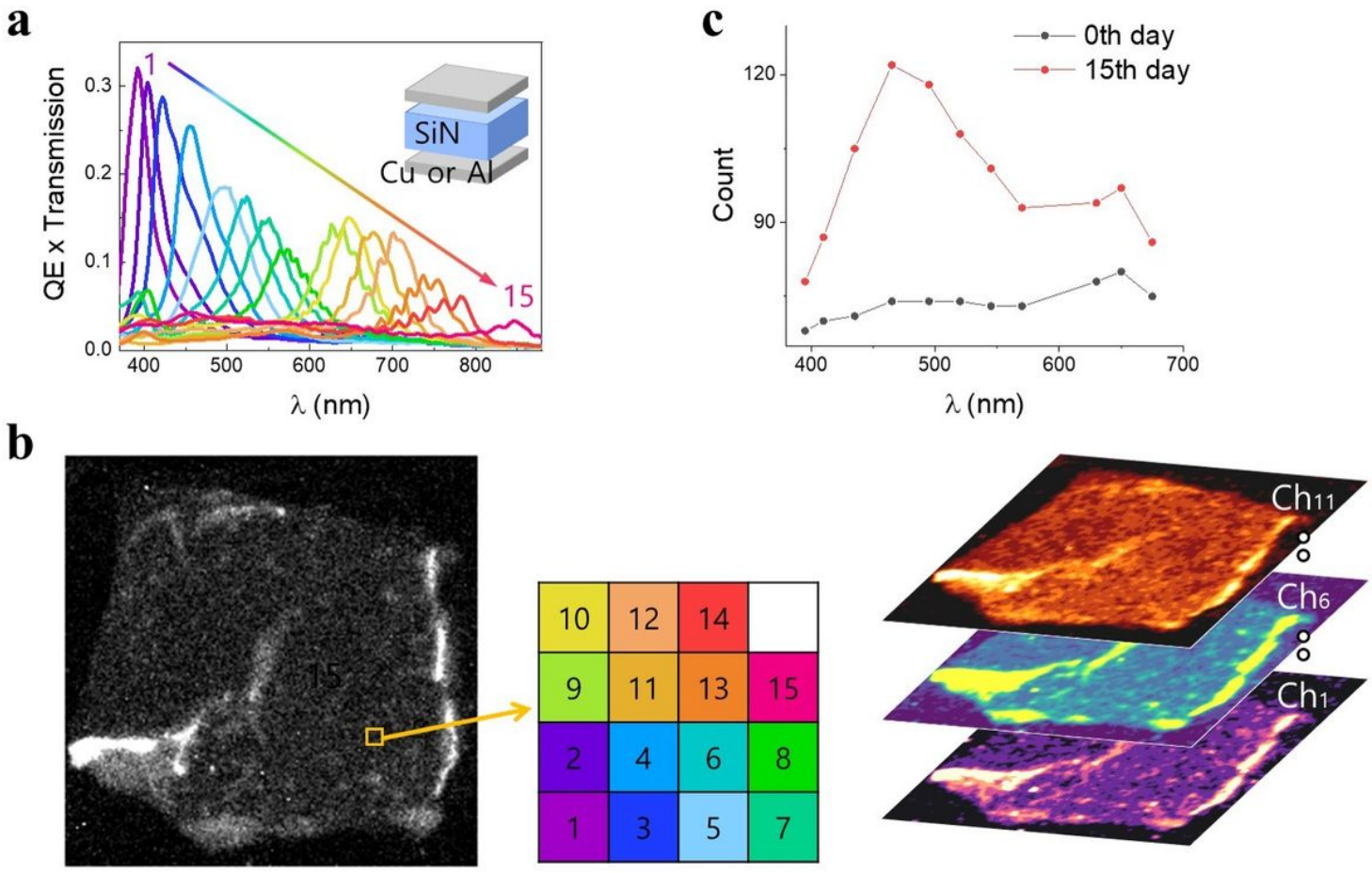

Figure 4

Hyperspectral image of meat fluorescence by snapshot-type HIS. (A) Characteristic curves of quantum efficiency multiplied by transmission of each channel. The inset is the schematics of the channel in the Fabry–Perot filter structure. (B) Hyperspectral image of the meat fluorescence excited by 365 nm LED. Fifteen channels of peak wavelength in the 380–850 nm range and one metal block (4´4 channels) are periodically arranged as indicated in the illustration on the right-hand side. Each color represents the channel's peak wavelength in accordance with the color of the characteristic curves in (A). Three representative demosaiced hyperspectral images on the 1st, 6th, and 11th channel of which center wavelengths are 390, 524, and 675 nm are shown. (C) Spectrum extracted from the hyperspectral images obtained on the 0th and the 15th day for the PE-wrap-packaged specimen, which were in the fresh and rotten state, respectively.

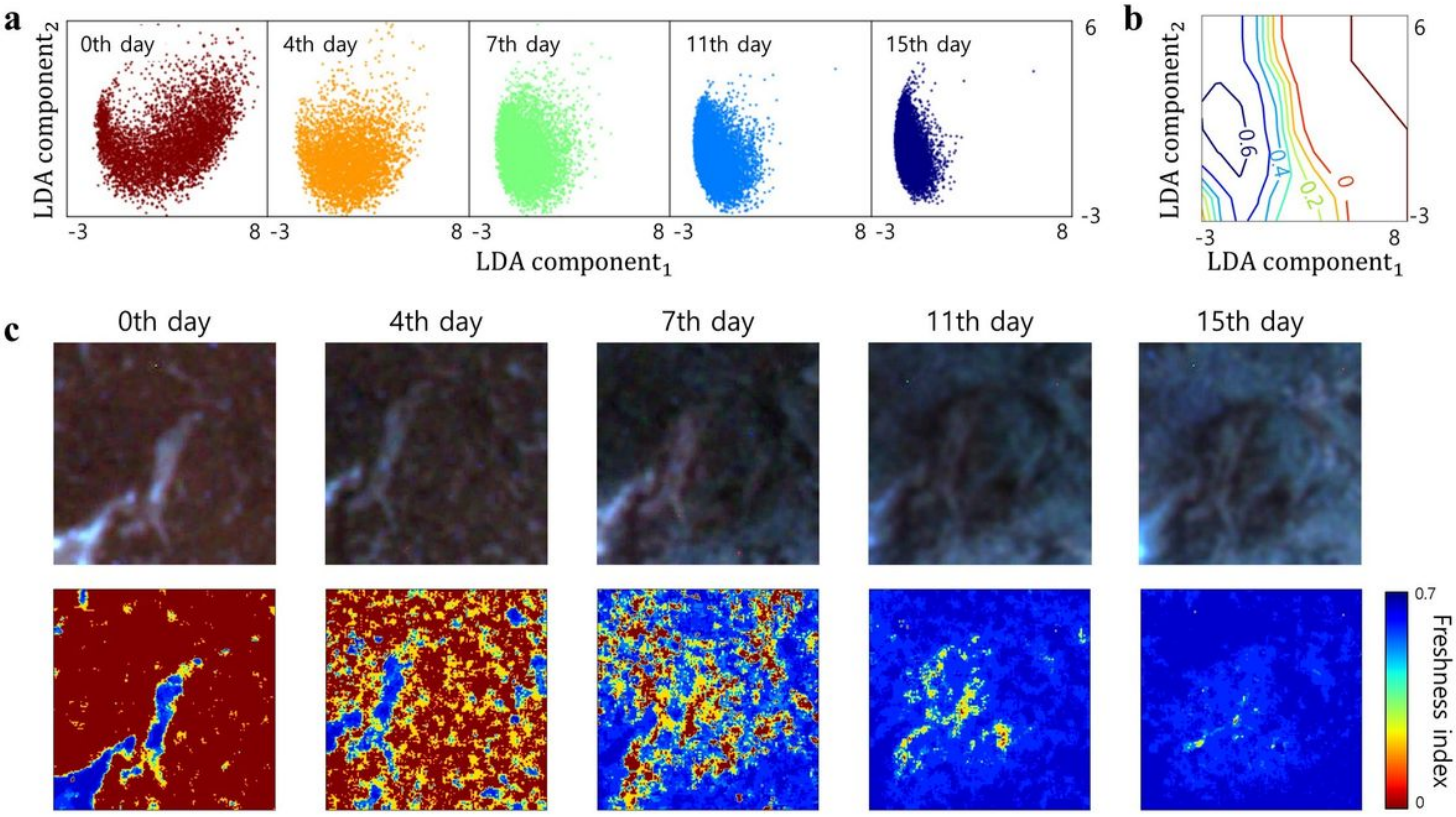

Figure 5

ML for evaluation of meat freshness.(A) LDA components, which are a result of dimension reduction from 11 to 2 for analyzing meat freshness from hyperspectral images of the meat fluorescence. The images are obtained by snapshot-type HIS and two-dimensional maps at five representative storage times. (B) Decision boundary contour determined by QDA to find F. I. Meat freshness at unknown state was evaluated by LDA and QDA of the hyperspectral images of the meat fluorescence. Numbers inside the contour plot are from the F. I. values obtained from the scan-type hyperspectral image of the same meat specimen. (C) Upper panels are the RGB images converted from the hyperspectral images at five representative storage times. The two-dimensional maps of F. I. for the RGB images are displayed at the lower panel.

Supplementary Files

This is a list of supplementary files associated with this preprint. Click to download.

- ExtendedDataFigsandTable.docx